

# SINGLE SHOT TRANSVERSAL PROFILE MONITORING OF ULTRA LOW CHARGE RELATIVISTIC ELECTRON BUNCHES AT REGAE

H. Delsim Hashemi\*, DESY, Hamburg, Germany

## Abstract

Relativistic electron microscopes are increasingly under consideration in dream experiments of observing atomic scale motions as they occur. Compared to ordinary electron microscopes that are with energies limited to few tens of keV, relativistic electrons reduce the space-charge effects strongly. This enables packing more electrons in shorter bunches and thereby capturing atomic scale ultra-fast dynamics even in a single shot. A typical relativistic-electron-microscope, based on an RF-gun, can provide experiments with couple of thousands to millions of electrons bunched in a few  $\mu\text{m}$  length and a transversal dimension of a fraction of a mm. After scattering from a sample diffracted electrons are distributed over transversal dimensions typically two orders of magnitude larger. For transversal diagnostics before scattering a cost effective solution is implemented while for Diffraction Pattern (DP) detection the goal is imaging the entire pattern with single-electron imaging sensitivity and good signal to noise in single shot and keeping well depth as high as possible.

## INTRODUCTION

Beam quality demands for relativistic electron microscopy are extraordinary. To study e.g. proteins a coherence length of 30 nm is required which translates into a transverse emittance of 5 nm at a spot size of 0.4 mm. In order to study chemical reactions or phase transitions in pump-probe experiments short bunch lengths down to 10 fs and a temporal stability of the same order are required. These are challenging parameters for an electron source, which can only be reached at a low bunch charge of about 100 fC [1]. REGAE (Relativistic Electron Gun for Atomic Exploration) has been commissioned at DESY with the goal to produce electron bunches as required for electron diffraction [2]. REGAE employs a photocathode S-band RF gun that operates at high accelerating fields providing means to suppress space charge induced emittance growth. Space-charge forces that limit the density of electrons too, scale inversely with the energy of electrons squared. This explains the advantage of relativistic electrons. The draw back for scintillator base transversal diagnostics is the reduction of energy loss in a typical energy of 5 MeV. This fundamental problem makes it challenging to image relativistic-electrons. Radiation damage is another draw back with relativistic-electrons.

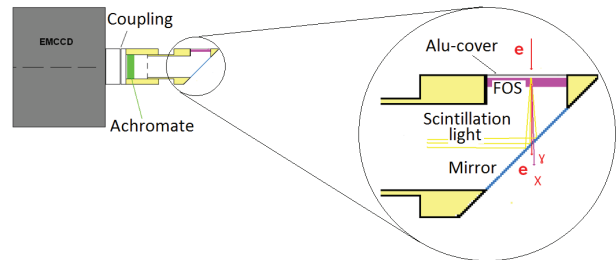


Figure 1: Schematic layout of DP-detector. Electron beam hits the 150  $\mu\text{m}$  thick CsI scintillator of FOS in normal angle and generates the scintillation light that gets coupled efficiently to the fiber optics. The image that is formed at the exit of fiber plate is reflected by a mirror towards the camera. This mirror is transparent for x-rays and energetic electrons and reflects the scintillation light to the coupling optics of the camera.

## INDIRECT DIAGNOSTICS USING SCINTILLATORS

Due to high radiation damage in the energy range of 3 to 5 MeV direct electron detection is not an option. Here scintillators can be used to make a copy of electron-beam transversal profile. Geometrically there are two ways to use a scintillator to detect the transversal distribution of electrons; transmissive and reflective. In transmissive option usually scintillator is perpendicular to the electron beam and the light generated in forward direction can be collected by a downstream mirror. This mirror can be a metal coated thin silicon wafer. Such mirror can be transparent for electrons and x-rays and reflect visible scintillation light to be coupled to a camera, see Fig. 1.

In reflective geometry, scintillator is held with  $45^\circ$  to the electron-beam axis and backward scintillation light is lens coupled toward a camera. This is mainly used for diagnostics at injector part of REGAE [3].

### Detection System Parameters

For an electron-imaging system,  $N_e$ , the total number of electrons generated in one pixel can be expressed as a function of the performance characteristics of the various detection-system parameters. For a lens coupled CCD it can be written as:

$$N_e = n_e \eta g QE \quad (1)$$

where  $n_e$  is the number of electrons per unit area (e.g. the area on the scintillator that is imaged to a pixel of the CCD),

\* hossein.delsim-hashemi@desy.de

$\eta$  is the number of visible photons generated in scintillator per electron,  $g$  is the optical coupling efficiency and QE is the quantum efficiency of CCD. It is clear that a scintillator with higher light-yield, a more efficient geometrical coupling and higher CCD quantum efficiency are beneficial. Scintillator light-yield and quantum-efficiency of CCD are both function of wavelength thus, matching should be taken into consideration as much as possible. Using a back illuminated cooled chip Electron Multiplying Charge Coupled Device (EMCCD; e. g. Andor iXon3-DU-888-EC-BV [4]) can provide a  $QE \approx 0.9$  for an emission which has its peaks around green light. The optimization of the other two factors namely  $\eta$  and  $g$  is coupled to the resolution of the detector system and mechanical design constraints. The number of generated photons per passage of electron can be increased with thicker scintillator but thicker scintillator ruins out the resolution. State of the art x-ray detector Fiber Optics Scintillator (FOS [5]), can be used to generate considerably high number of visible photons, in forward direction, that can be coupled to fibers resulting in a good detection-efficiency and resolution. The angular spread of the light at the output of FOS is not Lambertian and features a sharp peak in the forward direction. This results in an improved optical coupling efficiency to the CCD.

### Geometrical Coupling Efficiency

Define  $F(\theta)$  as:

$$F(\theta) = \int_0^\theta f(\theta') \sin(2\theta') d\theta' \quad (2)$$

where  $f(\theta)$  is the normalized angular distribution of the radiance of the scintillator and  $\theta$  is the meridian angle,  $g$  can be written as:

$$g = T \frac{F(\theta_{max})}{F(\pi/2)} \quad (3)$$

with  $T$  being bulk transmission of the optical setup [6–8]. Applying this formalism to FOS and an ordinary Lambertian scintillator one can see that with FOS coupling efficiency is considerably higher.

In order to optimize collecting optics knowledge of spatial distribution of scintillator emission is required. In general simulation tools can be used to deal with radiance problem provided enough optical data of the scintillator. A direct measurement of radiance would result in a way to cross check simulations and develop an understanding of different processes in scintillation. When a complicated situation like FOS is under study experimental result are necessary due to the complication that arise in simulation with the coupling of the emission to the fibers. Furthermore the aluminum coating that works as the shielding of the stray light and reflector for backward scintillation light makes the situation with FOS even more complicated to simulate.

ISBN 978-3-95450-177-9

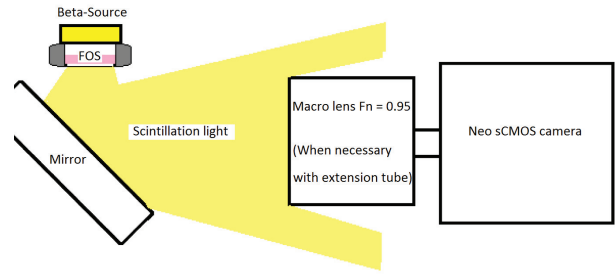


Figure 2: Layout of the setup to measure the radiance of FOS.

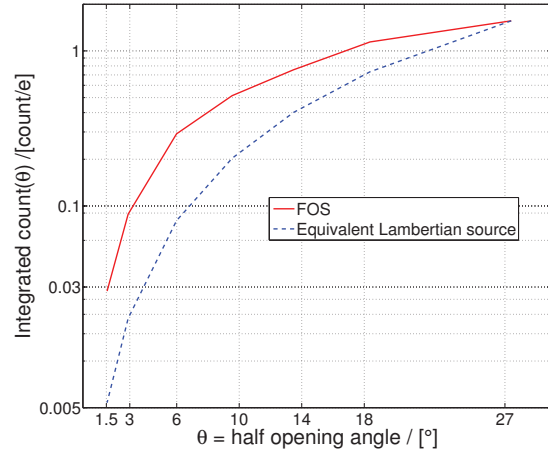


Figure 3:  $\beta$ -source is used to produce scintillation light and counts that scale with the collected light as a function of distance to the FOS are shown. For comparison a Lambertian source radiance is also shown that adjusted to emit the same amount of light into largest cone covered in the closest distance to the FOS.

For the measurement a setup that is illustrated in Fig. 2 is used. Background is reduced considerably using a light tight black closure that houses the entire setup. In the analysis the still remaining background as well as read-out offset and contribution of bad-pixels are removed by using signal minus background shots. At different distances from source a sharp focus is first achieved and then background ( $T$  seconds exposure without source, typical  $T = 100$  seconds) is recorded. Then source is placed in and signal shots are recorded exposing again  $T$  seconds. As camera Neo sCMOS [9] cooled to  $-35^\circ$  is used. Integrated counts over the ROI (background removed) is proportional to the collected light and as a function of distance is shown in Fig. 3 for FOS. For comparison the radiance of a properly adjusted Lambertian source is also plotted. It is well known that the total intensity emitted into half opening angle  $\theta$  in forward direction for a Lambertian source is given by the integral:

$$f(\theta) = \pi f(0) \int_0^\theta \sin(2\theta') d\theta' \quad (4)$$

Where  $\theta$  varies between 0 and  $\pi/2$ . In order to make a sensible comparison instead of full hemisphere, integration can be limited to the maximum angle that was covered by FOS setup in the closest distance to  $\beta$ -source (largest opening angle of  $27^\circ$ ). Then it is set equal to the integrated counts for the FOS and extracting the resulted constant,  $f(0)$ , for maximum luminance in normal direction the functionality of Lambertian source is derived. Given the realistic situation in accelerator diagnostics setup in terms of vacuum window aperture size etc. FOS collection is close to an order of magnitude higher than a Lambertian scintillator. In many studies simplified forms of Eq.3 and Eq. 2 for Lambertian or point source are used [8]. The real  $g$  can be only deduced from integration of radiance, like what is derived here experimentally and shown in Fig. 3, in Eq. 3. As it is clear from Fig. 3 FOS output in backplane is neither like a point source nor Lambertian.

### DETECTIVE QUANTUM EFFICIENCY (DQE)

Assuming that  $n_e$  in Eq. 3 follows Poisson's statistics the intrinsic signal to noise ratio reads as  $\sqrt{n_e}$ . This means that the input signal introduces an upper limit to detection efficiency. DQE can be defined as [10]

$$DQE = \frac{(S/N)_{out}^2}{(S/N)_{in}^2} \quad (5)$$

One can describe DQE as a generalization of camera quantum efficiency to include the statistical behavior of electron to photon conversion in scintillator and photon to electron in camera chip as well as statistical behaviour of amplification process in camera electronics. Even for an ideal camera with  $QE = 1$ , DQE can be smaller than one, because the conversion to scintillation photons introduces a statistical noise among all other contributions. The DQE can be considered as the fraction of incident events that are registered by the detection system. As higher DQE is as shorter exposure of events is needed to get the same quality image and information. Detector setups composed of scintillator, coupling optics, intensifier or electron multiplier and camera can be compared by measuring DQE. For such comparisons with same  $n_e$  measuring either DQE or  $(S/N)_{out}$  is the same. DQE can be used to compare detection systems that are prepared to work at different  $n_e$  level. Furthermore effects like coupling optic differences from a setup to another results in changes in total number of photons coupled to the camera chip that can be unfolded when DQE is used.

In order to measure DQE one needs a source that is as stable as possible. This is why a  $\beta$ -source is chosen with activation in the range of 2.4 MBq. Here the two detectors that are operational at REGAE will be considered. One is based on an EMCCD [4] lens coupled to FOS (called in the following D1) and the second one is a Neo sCMOS lens-coupled to a Photek large area image-intensifier [11] that gets its input

again lens-coupled from FOS (called in the following D2). For both detectors the number of electrons is controlled by exposure time of FOS to the  $\beta$ -source. For D1 two case with EM-gain of 50 and 300 are examined. EM-gain of 300 is maximum ordinary gain where EMCCD shows the highest sensitivity to the extreme low light intensities and EM-gain of 50 is a moderate value. With D2 one case with the same number of electrons per pixel as of D1 experiments and another one with lower electrons per pixel are acquired which the latter fits the best to the maximum gain applied to the intensifier. For any of these four measurements a background, a background subtracted signal (call it reference) and finally a series of 50 shots of signal are measured. From reference shot one can obtain  $\sigma$  of the spot assuming a Gaussian profile. Then the total counts in the reference can be extracted that corresponds to the total particle number exposed to the FOS (integrating over  $3\sigma$ ). Selecting a central spot of one- $\sigma$  size one can read the counts in reference image and background. As the next step the integral count in the one- $\sigma$  long central region is taken for all signal shots and the corresponding background count is subtracted from them. Mean value of these one- $\sigma$  long signal minus background and their standard deviation can be used to deduce the  $(S/N)_{out}^2$ . From the total integrated count and total integrated count over the ROI and activation of the  $\beta$ -source and the applied exposure time one can get  $(S/N)_{in}^2$  (assuming Poisson statistics). In Table 1 the results are summarized. D1 is in operation since 2012 and has provided means to

Table 1: DQE for REGAE Detectors

Detector	EM-gain	$\langle e/pixel \rangle$	DQE
D1	50	2.4	0.17
D1	300	2.4	0.15
D2	-	1	0.72
D2	-	2.25	0.6

record diffraction patterns from experiments with low intensities reaching to the aim of single electron per pixel detection in single shot. One typical result is shown in Fig. 4 (that will be discussed later). D2 is a new detector that can provide experiments with much better detectability as is shown in Table 1. The possibility of higher number of full resolution (5.5 MPixels) frames per second reaching to 38 with highest bit depth of 16 bits is demonstrated in commissioning. With highest gain of intensifier at D2 it is possible to image patterns that have single electron feature detected with good signal to noise ratio and a well depth up to 140 electrons per pixel. Well depth can be increased when sensitivity level is compromised. Another advantage of D2 in comparison to D1 is the short gating time that can be achieved. It is possible to gate down to 50 ns the Photek intensifier then there will be an improvement compared to D1 why an EMCCD needs several ms exposure to capture a shot thus suffering from contribution of dark-charge as will be explained later.

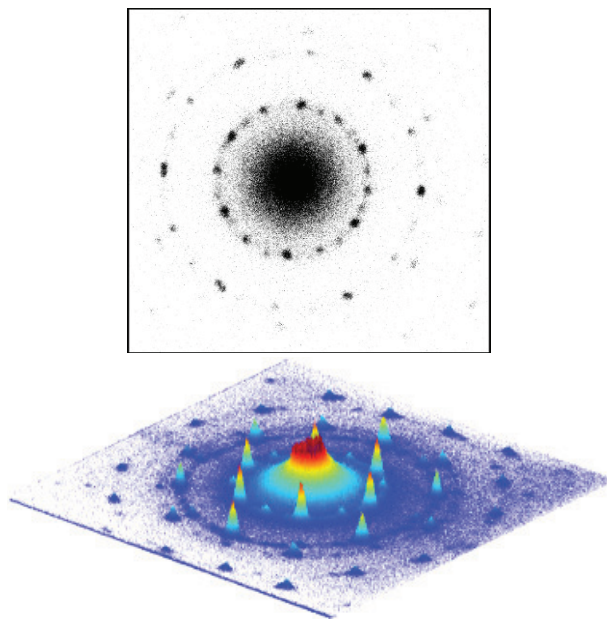


Figure 4: Top: 6 fC total charge is diffracted by a sample and resulted diffraction pattern is recorded in single shot. Bottom: Averaged over 200 shots like in the top.

## DIFFRACTION PATTERN DETECTION

D1 employs the transmissive scintillator geometry, see Fig.1. The core of the converter layout is composed of an FOS. This FOS is oriented perpendicular to the electron beam thus the Scheimpflug effect is corrected. A thin silicon-wafer coated with aluminum couple scintillation light to the collecting optics. This mirror acts as the reflector for the visible scintillation light and is transparent to the energetic-photons (namely X- or  $\gamma$ -rays) or relativistic electrons. The Si-wafer is  $100\mu\text{m}$  thick therefore practically no relativistic electron gets reflected backwards. The entire setup is in UHV of the accelerator and at the same time fully light tight such that no background photon enters to the detector setup (see Fig. 1). Lens coupling is done by a relay optics composed of two achromates (50 mm diameter) that image, with required de-magnification of  $\approx 0.8$ , the output of FOS to the camera chip. The entire FOS and coupling mirror are designed such that they can be moved into/out-of the beamline. D2 is installed downstream D1 and is a fixed installation.

### Experimental Results

In one of many diffraction experiments conducted at RE-GAE, electron bunches of a total charge 6 fC were used to get single shot diffraction images as Fig. 4-top using D1 detector. In each shot about 35 fC dark-charge contributes to the background. Dark-charge distribution varies from shot to shot. If one corrects for the shot to shot transversal jitter a superposition of many shots can improve the con-

trast of diffraction pattern against dark charge. After corrections are applied what contributes in the readout count, apart from diffraction orders, are the EMCCD read-out offset and hot spots of dark-charge. By subtracting this offset one can derive a calibration taking the advantage of in operation precise charge measurement diagnostics at RE-GAE [12]. Off-set of the image can be estimated using areas of the image that are far from any diffracted orders and hot dark current spots. The background and off-set free

Table 2: Electron Distribution in Different Orders

Order. no.	Intensity %	no. of electrons	no. of pixels	$\langle e/pixel \rangle$
0	92	33000	57256	0.58
1	5.1	1850	8010	0.23
2	2.84	1025	9125	0.11

integral count in all diffraction orders area and total charge can be used to deduce the absolute calibration that also will result in an estimation of dark charge. In Fig. 4-bottom, 200 shots are aligned and averaged. Using this image one can get percentage of the total charge that diffracts into individual different diffraction orders. As it is clear from image, detectability varies as a function of number of electrons that are diffracted into orders. For single shot at the top of Fig. 4 the number of electrons per pixel (with area  $13 \times 13 \mu\text{m}^2$ ) is fraction of electron (see Table 2).

## ACKNOWLEDGMENTS

This work is supported by many groups at DESY, HASYLAB and CFEL and individuals including D. Gitaric, S. Bajt and M. Spiwek.

## REFERENCES

- [1] M. Hada et al., Opticsinfobase online publication JT2A.47, ICUSD2012.
- [2] S. Manz et al., Faraday Discussions, Volume 177, 2015.
- [3] Sh. Bayesteh et al., proceedings IBIC 2013, MOPF06.
- [4] <http://www.andor.com/scientific-cameras/ixon-em-ccd-cam-era-series>
- [5] <http://www.hamamatsu.com/jp/en/J6677.htm>
- [6] W. Swindell, Med. Phys. 18, 1152-1153 (1991).
- [7] Tong Yu and John M. Boone, Med. Phys. 24(4), April 1997.
- [8] Hong Liu et al., Med. Phys. 21(7) July 1994.
- [9] <http://www.andor.com/scientific-cameras/neo-and-zyla-scmos-cameras/neo-55-scmos>
- [10] Mark W. Tate et al., Rev. Sci. Instrum. 68(1), January 1997.
- [11] <http://www.photek.com/pdf/datasheets/detectors>
- [12] D. Lipka et al., proceedings IBIC 2013, WEPF25.